A scalable data driven approach to temperature baseline reconstruction for guided wave structural health monitoring of anisotropic CFRP structures

Nan Yue*, M.H. Aliabadi

Department of Aeronautics, Imperial College London, South Kensington Campus, City and Guilds Building, Exhibition Road, SW7 2AZ, London, UK

Abstract

To account for the temperature effect on guided wave signals in complex structures, a significant amount of baseline measurements typically need to be collected over a large temperature range to serve as a library of signals at all possible temperatures, which, if not impossible, is highly impractical. This paper presents a data-driven temperature baseline reconstruction approach that is applicable for various structures made from the same material. The influence of temperature on the amplitude and phase of guided wave measurements are experimentally quantified as dimensionless compensation factors. The derived compensation factors are used to reconstruct baselines at various temperatures for guided wave measurements in a simple flat plate and a stiffened panel. With a single baseline measurement at $20°C$ and the reconstructed baseline using the predetermined temperature compensation factors, impact damage was successfully detected and located when current measurements were up to $25°C$ and $20°C$ higher than the baseline temperature, respectively.

Keywords: Structural health monitoring; Guided waves; Thermal sensitivity; Temperature compensation; Composite laminates; Stiffened panel; Up-scaling; Piezoelectric sensor.

1. Introduction

Ultrasonic guided wave has been recognised as an effective tool for interrogating large structures due to its capability of propagating over long distances with small energy loss. Typically a Guided Wave Structural Health Monitoring (GWSHM) system utilises a network of piezoelectric transducers to excite guided wave and capture the guided wave signals. Detection of damage relies on interpreting the correlation between change of the signals and the characteristics of damage. In aircraft structures, where structural complexities such as multiple boundaries, stiffeners and openings are typical, guided wave signals inevitably contain multiple boundary scatters and reflections, which makes the captured signal difficult to interpret. In this case, pre-recorded measurements in a known integrity state of the structure serve as baselines for identifying deviations from the baseline measurements and can be related to the occurrence of damage.

Many effective GWSHM metholodies have been proposed and achieved successful application in controlled laboratory environmental conditions [1, 2, 3, 4, 5, 6, 7]. However, one of the major challenges of GWSHM to be readily applied on actual aircraft structures is achieving effective damage detection in uncontrolled environmental conditions. The most prominent and immediate change in guided waves is due to the thermal sensitivity of material properties. In aircraft service environments, temperature typically varies from -50°C to 50°C. Deviation

*Corresponding author
Email addresses: nan.yue14@imperial.ac.uk (N. Yue), m.h.aliabadi@imperial.ac.uk (M.H. Aliabadi)

in guided waves from the baseline caused by temperature changes can often mask the change in guided wave caused by occurrence of damage, dramatically decreasing the effectiveness of damage detection. In order to achieve reliable damage diagnostic using GWSHM in typical service conditions, the effect of temperature on guided waves has to be compensated[8].

The first attempts to overcome varying temperature conditions involved building libraries of baseline signals covering a range of temperatures often encountered during service conditions. The optimal baseline is selected according to the temperature or the degree of similarity to the current signal [9, 10]. The baseline selection approach requires no prior knowledge of the temperature sensitivity of the materials but requires a large number of baseline signals to be recorded for each of the GWSHM systems, which is, if not impossible, very time consuming and requires a significant amount of data storage and management when a large number of sensors are utilised.

Later attempts to overcome varying temperature conditions used a baseline correction approach involving matching one signal to another by signal stretching. Lu and Michaels [9] investigated the effects of temperature on diffused-like guided waves in a small aluminium plate. Results showed that time delay in signal arrival time caused by temperature changes is linearly correlated to the time elapsed and is independent of the presence of a through thickness crack or a hole. This time delay was characterized by the slope of the time delay as calculated from the short time cross correlation between two signals recorded at different temperatures. To compensate for this time delay, the signal was stretched or compressed by modifying its time axis. Croxford et al. [10] proposed a similar signal correction technique that modifies a baseline waveform by compressing or dilating the waveform using a stretch factor to match the current waveform. The optimal stretch factor was obtained via an iterative algorithm that yielded the stretch factor minimising the mean squared deviation or the maximum residual amplitude of the residual signals. Instead of altering the time-axis, the waveform stretch was achieved by transforming the signal to the frequency-domain using Fast Fourier Transform (FFT) and modifying the corresponding portion of the frequency spectrum. The modified frequency spectrum is then converted back to the time-domain using inverse FFT. Harlay et al.[11] employed scale transform for signal resampling and showed improved computational speed over FFT. Dworakowski et al.[12] achieved signal alignment of two signals with an alternative method. The Hilbert transform was implemented to obtain analytic signals and to extract their instantaneous phase. The time delay between two signals was compensated by aligning their instantaneous phases. Although this method eliminates all time shift caused by temperature change, it might also remove the local phase change caused by a damage scattered wave, potentially making it more difficult to detect the damage. All of the above baseline correction methods are based on computing the optimal stretch factor to achieve the best match between the baseline and the current measurement, and therefore require significant computational effort.

More recent attempts utilize a data driven approach for temperature compensation. Liu et al.[13] proposed a method to reconstruct baseline waveforms at the temperature of current measurement. Two baseline waveforms measured at different temperatures were utilised for the reconstruction. The phase of the baseline waveforms were extracted using Hilbert transform. The phase of the reconstructed signal was determined using linear interpolation with the phase of the two baseline waveforms. The amplitude of the reconstructed waveform was determined using Orthogonal Matching Pursuit (OMP) to match the current measurement. However, the correct interpolation of phase was difficult to achieve in the presence of cross-talk and random noise at the beginning of the signal.

Di Scalea and Salamone [14] developed an analytical model to predict the S0 and A0 mode guided wave response spectra in an isotropic plate for the temperature range of $-40°C$ to $60°C$. The model combines the piezomechanical properties of the actuator and the sensor, the interaction between the actuator and sensor with the substrate plate through shear-lag behaviour, and the guided wave dispersion in the plate. Inspired by this, Roy et al. [15] developed a temperature compensation model for guided wave responses acquired with piezo-sensors on aluminium plates. The assumption of linearly varying phase-shift was abided by. Matching Pursuit (MP) decomposition was implemented to characterise and reconstruct guided wave response at different ambient temperatures. A data driven approach to temperature compensation for a composite plate was proposed by Fendzi et al.[16]. The change in amplitude and phase of a signal due to temperature change was extracted using the Hilbert transform and described using Least square regression models. However the structure considered was a simple plate with quasi-isotropic layup, the adaptation of the temperature compensation strategy in more complex aircraft composite structure remained unaddressed.

Most of the aforementioned temperature compensation methods [9, 10, 11, 12, 15] were developed for isotropic materials where the temperature effect is considered to be the identical in all directions, which are not adequate for anisotropic material such as carbon-fibre composite laminates. Those method developed for anisotropic materials [16] only considered simple structure and was not applied in large-scale structures. An effective temperature compensation strategy for guided wave temperature compensation in anisotropic composite materials should not only consider the anisotropy of temperature effect but also be readily scalable for various transducer layout in large and complex structure.

This paper presents a physically based baseline reconstruction approach to compensate the temperature effect on GWSHM for anisotropic composite structures. The temperature effect on guided wave response is investigated experimentally in multiple directions. The change in signal amplitude and arrival time is quantified as dimensionless compensation factors and is estimated using least squares regression for a large temperature range in all wave propagation directions. Baseline signals at different temperature are reconstructed from a baseline signal at one temperature using the estimated dimensionless compensation factors. The baseline signals can be reconstructed for different sensor layout in structures made from the same material. The proposed baseline reconstruction approach is implemented in damage characterisation of two typical aerospace composite structures, a simple flat panel and a stiffened panel.

2. Theoretical framework

In this work, we consider guided wave actuating and sensing using surface bonded piezoelectric transducers in a pitch-catch configuration. Ultrasonic guided wave is actuated in plate structure using piezoelectric transducer and the propagating disturbance is measured at distributed piezoelectric transducers as voltage signals.

2.1. Influence of temperature on signal phase

Consider a change of the signal if there is a change in temperature $T = T_0 + \delta T$. Signals can alter in amplitude and shape because of possible temperature dependence of dispersion and attenuation mechanisms.

Due to the dispersive nature of guided wave, temperature changes cause the change in both phase velocity and group velocity. The latter changes the time of arrival of a wavepacket and the former changes the phase of the signal within the wavepacket. It is commonly acknowledged in the GWSHM community that the non-dispersive guided wave mode should be selected for the effective application. For simplicity, guided wave is

considered to be non-dispersive. In other words, we assume that guided wave retains the same waveform as it propagates.

Arrival time of a wave component is $\tau = r/v_p$, where r and v_p denote distance and velocity respectively. The change in arrival time caused by temperature deviation within the wave packet can be written as[17]:

$$\frac{\delta\tau}{\delta T} = \frac{1}{v_p}\frac{\delta r}{\delta T} - \frac{r}{v_p^2}\frac{\delta v_p}{\delta T} = \frac{r}{v_p}(\frac{\delta r}{r\delta T} - \frac{\delta v_p}{v_p \delta T}) \tag{1}$$

Above equation as be rewritten as [17]

$$\frac{\delta\tau}{\tau} = (\alpha_L - \frac{k_{vp}}{v_p})\delta T \tag{2}$$

where $\alpha_L = \frac{1}{r}\frac{\delta r}{\delta T}$ denote linear thermal expansion coefficient, $k_{vp} = \frac{1}{v_p}\frac{\delta v_p}{\delta T}$ is the fractional change in phase velocity.

Assume the proportional time shift is linearly related to the change of temperature and is irreverent to the propagation distance. Denote β as the ratio between the new arrival time and original arrival time

$$\beta = \frac{\tau + \delta\tau}{\tau} \tag{3}$$

Substitute Equation (2) into Equation (3) we have

$$\beta = 1 + (\alpha_L - \frac{k_{vp}}{v_p})\delta T \tag{4}$$

Note α_L, k_{vp} and v_p are material properties and can be determined experimentally. In this work β is considered as a material property and is obtained experimentally using Equation (3).

2.2. Influence of temperature on signal amplitude

The sensor voltage output V_{out} can be expressed as a function of actuator input voltage V_{in} as[15]:

$$V_{out} = d_{31}C_{act}C_{sen}\frac{d_{31}E}{\epsilon_{33}(1-\nu)}V_{in} = DV_{in} \tag{5}$$

where d_{31} is the piezoelectric actuation coefficient, C_{act} and C_{sen} represent the shear lag properties of the actuator and the sensor, ϵ_{33} is the relative dielectric permittivity, E and ν are the piezoelectric Young's modulus and Possion's ratio in planer direction, respectively.

The attenuation coefficient of guided wave amplitude at distance r away from actuation can be described as[18]

$$C(r) = c_0\frac{1}{\sqrt{r}}e^{-\eta r} \tag{6}$$

where $\frac{1}{\sqrt{r}}$ describes the geometrical spreading and $e^{-\eta r}$ describes material damping, c_0 is a constant. The damping coefficient η can be determined as[19]

$$\eta = \frac{ln(\frac{A_0\sqrt{r_0}}{A_1\sqrt{r_1}})}{r_1 - r_0} \tag{7}$$

where A is wave amplitude and r is the distance from the actuator to the sensor, index 0 denote the sensor that is closer to the actuator and index 1 denote the sensor that is further from the actuator. Material damping might be small in metallic materials and thus neglected, however it has to be considered in viscoelastic materials such as fibre reinforced polymer composites [19, 18, 20]. Therefore, combine Equation (6) with (5) we have:

$$V_{out} = DC(r)V_{in} \tag{8}$$

The guided wave signal amplitude at temperature T and at another temperature $T + \delta T$ can then be represented as

$$V_{out}(T) = D(T)C(r,T)V_{in} \tag{9}$$

$$V_{out}(T+\delta T) = D(T+\delta T)C(r,T+\delta T)V_{in} \tag{10}$$

Denote α as the ratio between the new amplitude and the original amplitude, from Equation (10) and (9)we have

$$\alpha = \frac{V_{out}(T+\delta T)}{V_{out}(T)} \tag{11}$$

Combine Equation (11) with Equation (6) gives

$$\alpha = \frac{D(T+\delta T)}{D(T)}\frac{C(r,T+\delta T)}{C(r,T)} = \frac{D(T+\delta T)}{D(T)}e^{[\eta(T)-\eta(T+\delta T)]r} \tag{12}$$

From Equation (12) we can see the ratio of wave amplitude in different temperatures is a function of piezoelectric properties and guided wave damping coefficient. Therefore, α is a combined material property of piezoelectric transducers, adhesive and the plate structure, which can be used for baseline reconstruction at different temperatures. In this work, α is determined experimentally using Equation (11).

3. Experimental setup

The CRFP structures used in this work are made of laminates consisting of 10 layers of M21/194/34%/T800S unidirectional prepreg, Hexcel (GB) in the layup of $[+45/-45/0/90/0]_s$. Figure 1 shows the flat panel fabricated to investigate temperature effect and to derive compensation factors. To study the orientation dependence of guided waves in this an-isotropic layup sequence, 13 piezoelectric transducers (DuraAct, PI Ceramics) were placed on the surface of the panel, one transducer was placed in the centre of the panel and the other transducers were places 70 mm away from the centre at every 30°. The transducers were bonded to the panel using two layers of 33 μm thick thermoplastic film that achieves uniform bondline and repeatable adhesion[21].

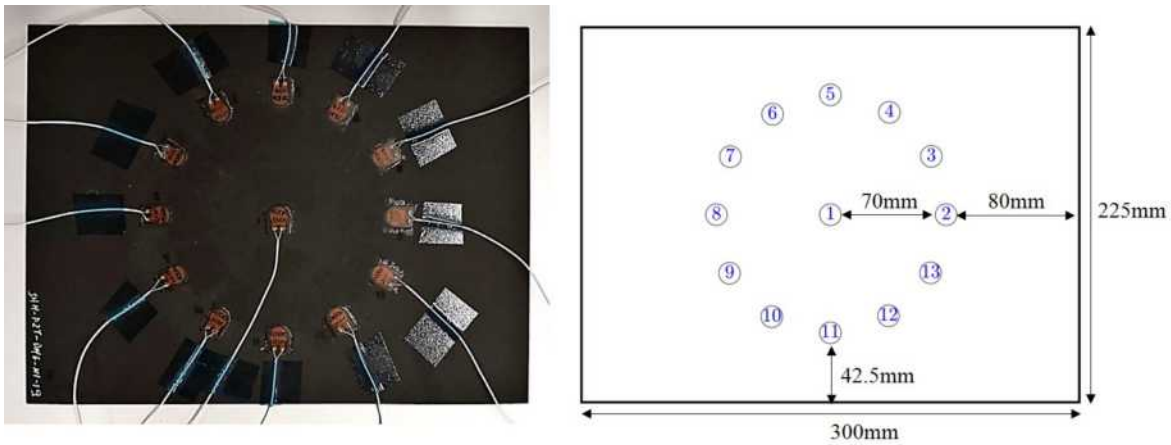

Figure 1: Panel A with 13 surface mounted DuraAct sensors

The panel was subjected to the controlled thermal conditions inside a thermal chamber (TVC J2235) while its guided wave responses were collected. The temperature inside the chamber was set to swipe from $-45°C$ to $65°C$ in steps of $5°C$. At each step, the temperature was held for 20 minutes to ensure that the panel reached the desired temperature before the guided wave measurements were taken.

Guided waves were excited in the panel using broadband chirp excitation signals for efficient acquirement of the guided wave responses over a range of frequencies [22]. The equation of broad band chirp excitation signal is

$$s^c(t) = w(t)\sin(2\pi f_0 t + \frac{f_1 - f_0}{T}t^2) \tag{13}$$

where f_0 and f_1 are the starting frequency and end frequency, respectively. T is the duration of the chirp. $w(t)$ is a rectangular window with user-set amplitude staring at $t = 0$ and end at $t = T$. A 12V peak-to-peak linear chirp excitation signal with frequency sweeping from 10 kHz to 600 kHz was applied to a piezoelectric transducer over a 200 μs window. The chirp response was recorded as the sensor output voltage signal with 60 MHz sampling frequency for the duration of 500 μs. The signals were collected in a round-robin manner, where one transducer acts as actuator and the others act as sensor until the signals from all the combinations of the transducers were collected.

The recorded chirp signal responses were deconvoluted to narrowband Hanning window toneburst response signals to enable interpretation in the time domain. The equation of Hanning window toneburst excitation signal is

$$s^b(t) = w(t)\sin(2\pi f_c t),\ w(t) = \frac{1}{2}[1 - \cos\frac{2\pi f_c t}{n_c}] \tag{14}$$

where f_c is the centre frequency, n_c is the number of cycles.

Response to toneburst excitation signal $s^b(t)$ was constructed from chirp response in frequency domain as [22]

$$R^b(\omega) = R^c(\omega)\frac{S^b(\omega)}{S^c(\omega)} \tag{15}$$

where R^c is the Fourier transform of measured response to chirp excitation $s^c(t)$, $S^b(\omega)$ and $S^c(\omega)$ are Fourier transforms of toneburst excitation $s^b(t)$ and chirp excitation $s^c(t)$ respectively. The toneburst response in frequency domain is then transformed to time domain obtained via inverse Fourier transform.

Symmetric mode (S0) dominant response to 3-cycle 250kHz toneburst excitation was observed, whereas anti-symmetric mode dominant (A0) response to 5-cycle 50kHz toneburst excitation was obtained. At these two frequencies, the amplitude and Time of Flight (TOF) of the first wavepacket of the toneburst reponse was obtained using the Hilbert transform. The group velocity was calculated as the ratio of the actuator-sensor distance to the corresponding TOF. Figure 2 shows the directivity of the amplitude and group velocity determined using transducer 1 as the actuator and transducer 2-13 as sensors at temperatures from -50°C to 65°C. While the direction dependence of both wave modes can be clearly seen, S0 mode shows greater variation in both amplitude and group velocity.

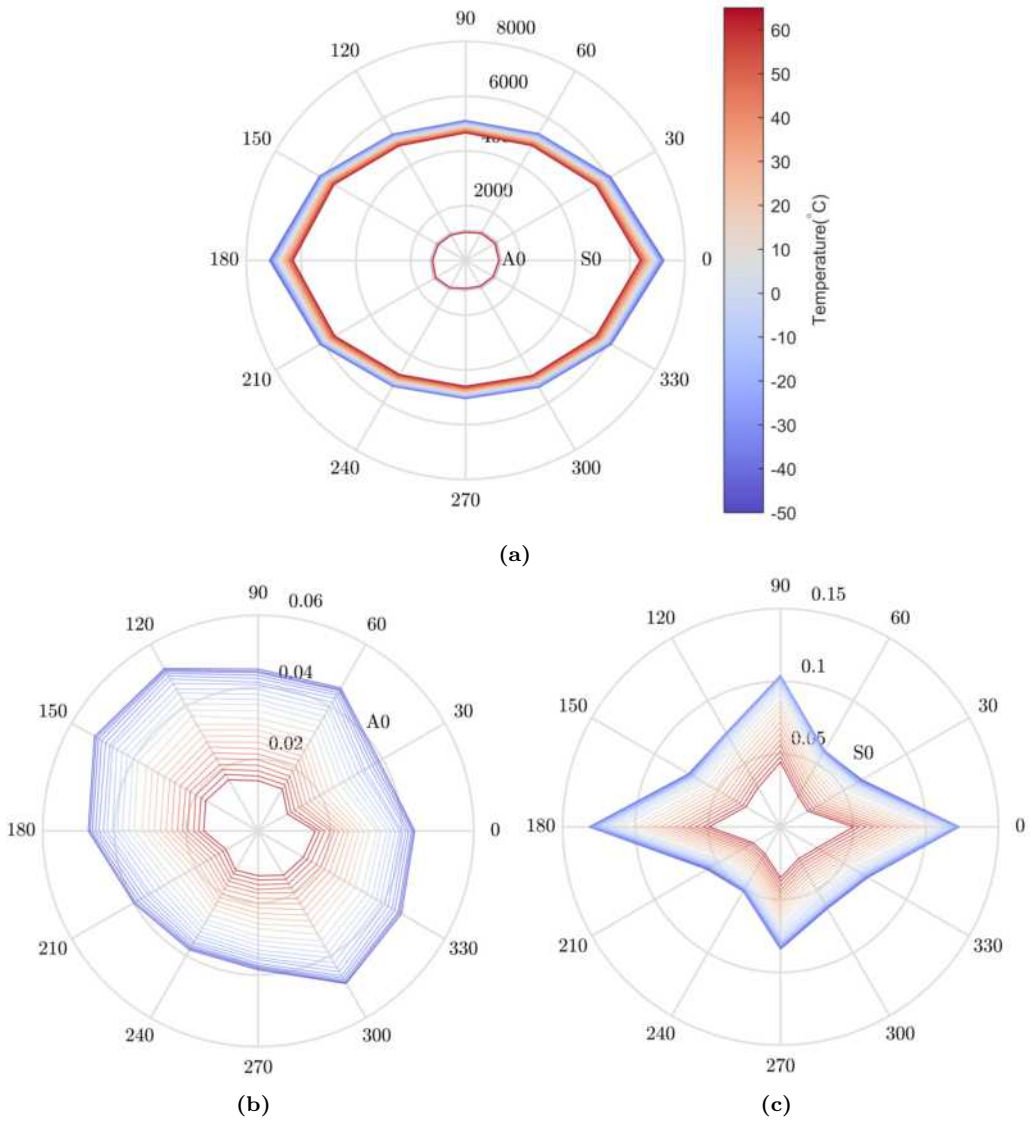

Figure 2: Directivity plot of guided wave signal characteristics of A0 mode response at 50kHz and S0 mode response at 250kHz: (a) group velocity (m/s) profile, (b) amplitude (V) of A0 mode response and (c) amplitude (V) of S0 mode response.

4. Physical based temperature baseline reconstruction

4.1. Signal feature extraction

This section proposes a waveform tracking approach to extract signal amplitude and phase from the first wave packet at various temperature conditions. Figure 3(a) presents the signal response to 5-cycle toneburst excitation over the temperature range from -50°C to 65°C. A number of crests and troughs within the first wave packet are located at the local maxima and minima using MATLAB function findpeaks, and are distinctly marked in Figure 3b. These marked points are used as the tracking positions of the waveform and need to be selected with care so that overlapping wave packets with cross-talk or later wave packets are excluded. The arrival time and the amplitude of the eight tracking positions within the first wave packet as a function of temperature are plotted in Figure 3(c) and 3(d). It can be seen that the arrival time of each tracking position increases almost linearly with temperature. The signal amplitude, however, declines with temperature at an accelerating rate and reaches a stable decline rate at around -10°C. Roy et al.[15] observed similar behaviour of signal amplitude. Ha et al.[23] suggested that the change of signal amplitude at different temperatures can be contributed primarily to the change in stiffness of the adhesive layer and the shift of resonance frequency of

the piezoelectric transducers. In order to eliminate the influence of crosstalk and the second wave packet on the signal features, only the second to the sixth tracking positions shown in Figure 3(b) are used for deriving the temperature compensation factors.

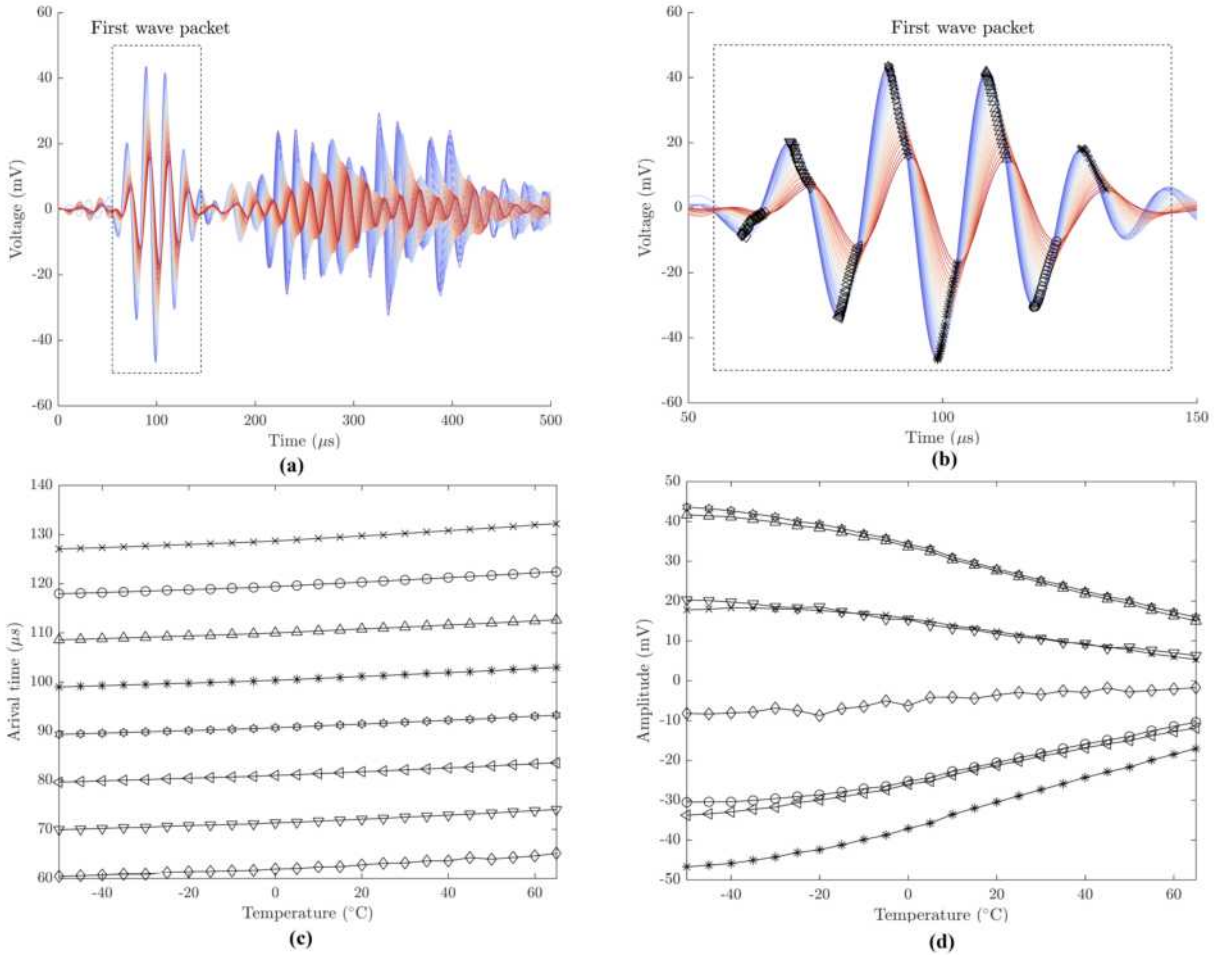

Figure 3: Signal feature extraction for A0 mode dominate response. (a) Signal response to 50kHz 5-cycle toneburst excitation recorded in path A1S2 on Panel A. (b) First wave packet at temperature from -50 to 65°C. (c) Arrive time of the tracking positions. (d) Amplitude of the tracking positions.

The same waveform tracking approach was used to extract signal amplitude and phase of S0 mode dominant signal response. Figure 4(a) presents the S0 mode signal response to 3-cycle toneburst excitation over the temperature range from -50°C to 65°C. In contract to A0 mode signal response to 5-cycles toneburst excitation shown in Figure 3(a), the first wave packet of the S0 mode signal response contains more crests and troughs despite the use of fewer toneburst excitation cycles, which indicates the more pronounced wave dispersion of S0 mode than A0 mode. The shape of the first wave packet of S0 mode also changes more significantly than A0 mode in varying temperature conditions, and the first wave packet of S0 mode signal becomes indistinct to the second wave packet as the temperature increase. Twelve possible tracking positions of the signal within the first wave packet are marked distinctly in Figure 4(b). It can be seen from Figure 4(c) that the shift in arrival time due to temperature variation becomes nonlinear for the later tracking positions. In order to capture and the signal features of the first wave packet only and suppress the effect of wave dispersion, only the second to sixth tracking positions are used for deriving the temperature compensation factors for S0 mode signal.

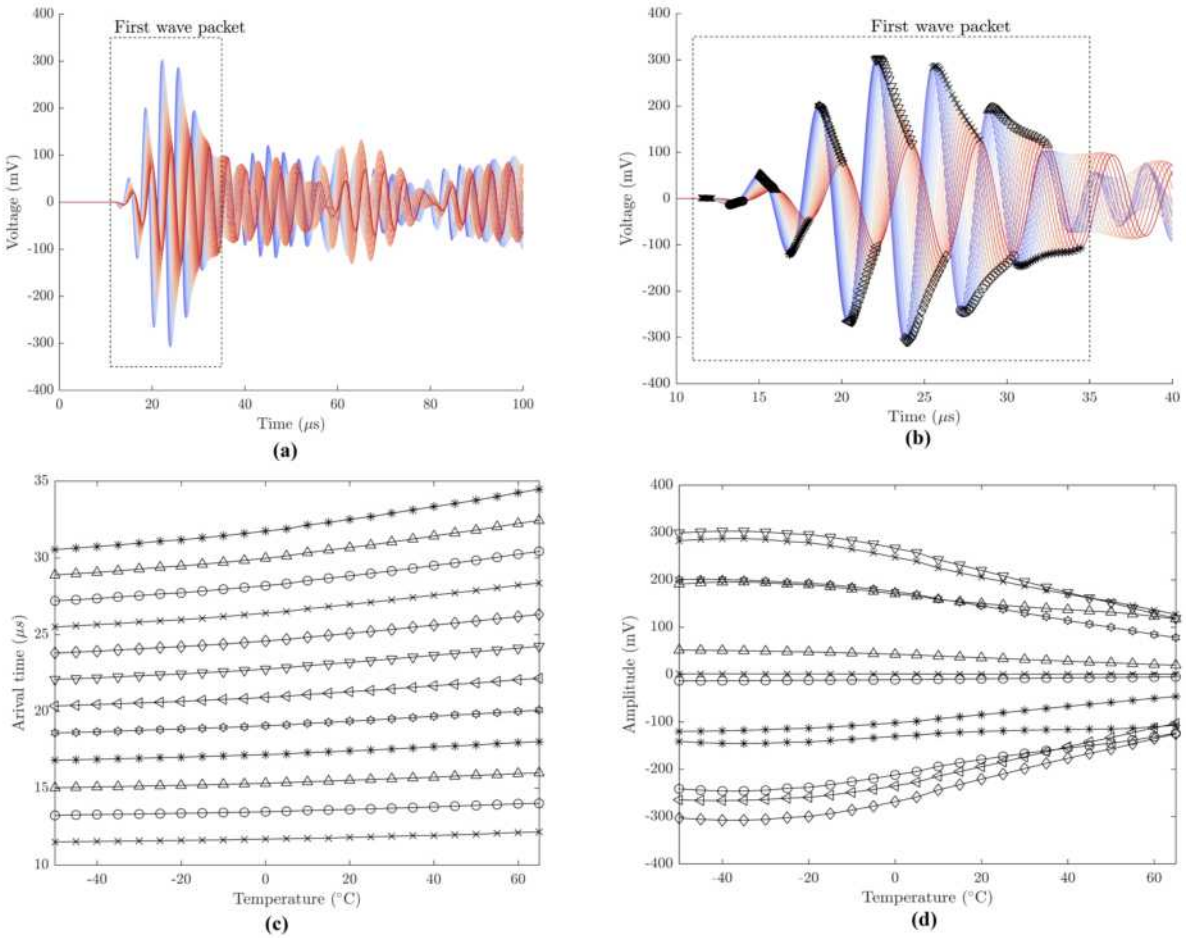

Figure 4: Signal feature extraction for S0 mode dominate response. (a) Signal response to 250kHz 3-cycle toneburst excitation recorded in path A1S2 on Panel A. (b) First wave packet at temperature from -50 to 65°C. (c) Arrive time of the tracking positions. (d) Amplitude of the tracking positions.

4.2. Polynomial regression

Amplitude and arrival time of the second to sixth tracking positions are used to obtain the amplitude ratio α and arrival time ratio β according to Equations (3) and (11), respectively, for the baseline temperature of 20°C. Figure 5 shows the obtained α and β values at from 50°C lower to 45°C higher than the baseline temperature. Both α and β show almost linear behaviour with respect to temperature deviation at both A0 mode and S0 mode dominant frequencies, 50kHz and 250kHz respectively.

Three polynomial models, linear, quadratic and cubic are used for least squares regression:

$$Linear : f^1(x) = ax + 1 + \epsilon \tag{16}$$

$$Quadratic : f^2(x) = ax^2 + bx + 1 + \epsilon \tag{17}$$

$$Cubic : f^3(x) = ax^3 + bx^2 + cx + 1 + \epsilon \tag{18}$$

where a,b and c are model parameters. The constant in each polynomial model is set to 1 as the compensation factors is 1 when temperature deviation is equal to zero. The model parameters of α is noted as $\boldsymbol{\theta}_\alpha, \boldsymbol{\theta}_\alpha = [a, b, c, ...]$. The model parameters of β is noted as $\boldsymbol{\theta}_\beta, \boldsymbol{\theta}_\beta = [a, b, c, ...]$. The model parameters are determined as:

$$\theta = argmin \sum [f(x_i, \boldsymbol{\theta}) - y_i]^2 \tag{19}$$

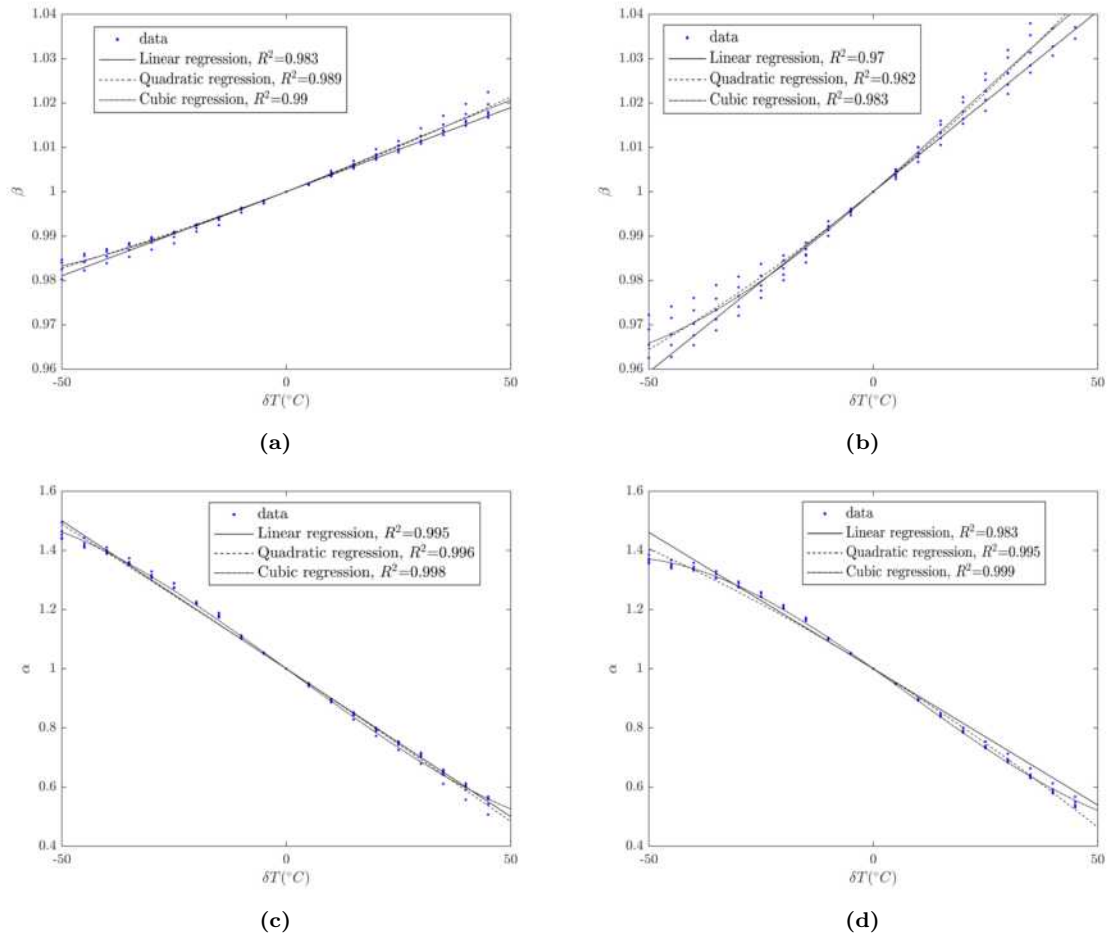

Figure 5: Least squares regression of and arrival time ratio β at (a) 50kHz and (b)250kHz, and amplitude ratio α at (c) 50kHz and (d) 250kHz.

The quality of fit of each polynomial model is evaluated by R^2 values and shown in Figure 5. Despite the considerable linear correlation of α or β with temperature deviation, the linear and quadratic models proved insufficient in describing the significant non-linear trends at the extremes of the temperature range. Thus the coefficients of cubic regression are used to derive the following results. It can be seen from Figure 5 that, for each δT value, the standard deviation of the arrival time ratio β values is greater for S0 mode than for A0 mode. It can also be observed that the mean β values for entire range of δT values have a wider range for S0 mode than for A0 mode. As discussed earlier in section 4.1, this is due to the more significant wave dispersion of S0 mode than of A0 mode.

Figure 6 shows the direction dependence of amplitude ratio α and arrival time ratio β for temperature deviation δT from -40°C to 40°C. The compensation factors in the orientation that is not present in Figure 1 are obtained using linear interpolation with the adjacent available orientations. It is evident that α and β values vary in different directions, which is as expected considering the anisotropic lay up and direction dependence of wave amplitude and velocity shown in Figure 2. Direction dependence of thermal effects on wave features in an-isotropic composite laminates might be further investigated with numerical simulations, but is out of the scope of this work.

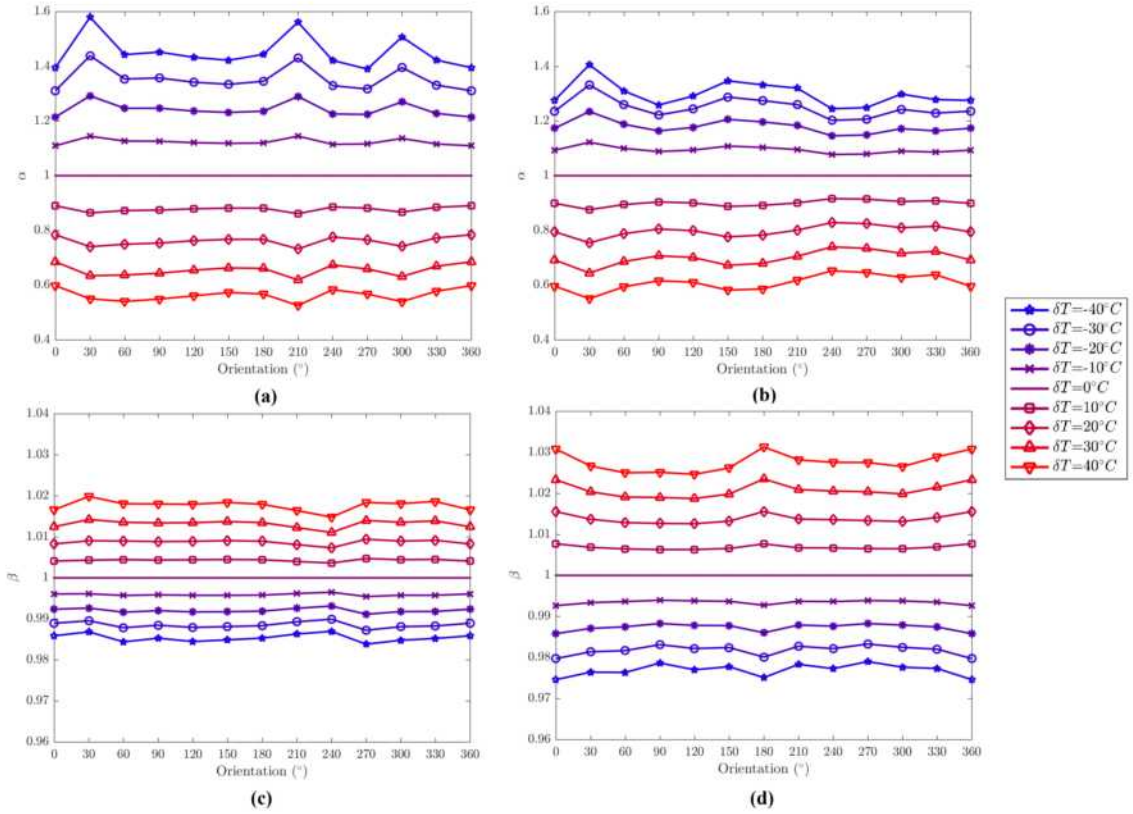

Figure 6: Direction dependence of compensation factors over a range of temperature with reference $T = 20°C$. Blue line colour indicates $\delta T < 0$. Red line colour indicates $\delta T > 0$. Amplitude compensation factor α at (c)50kHz (d)250kHz. Phase compensation factor β at (c) 50kHz (d) 250kHz.

4.3. Signal compensation

Temperature compensation of a signal at temperature T_0 for the temperature deviation of δT can be expressed as:

$$S_{T_0}(t) \rightarrow \alpha S_{T_0}(\beta t) \tag{20}$$

where the amplitude and arrival time compensation factors are derived from the regression model as $\alpha = f^3(\delta T, \boldsymbol{\theta})$ and $\beta = f^3(\delta T, \boldsymbol{\theta})$. The compensation of change in arrival time is achieved by multiplying the signal time vector by the arrival time compensation factor β and then linearly interpolating the signal in the original time vector. Change in signal amplitude is compensated by multiplying the signal vector by the amplitude compensation factor α.

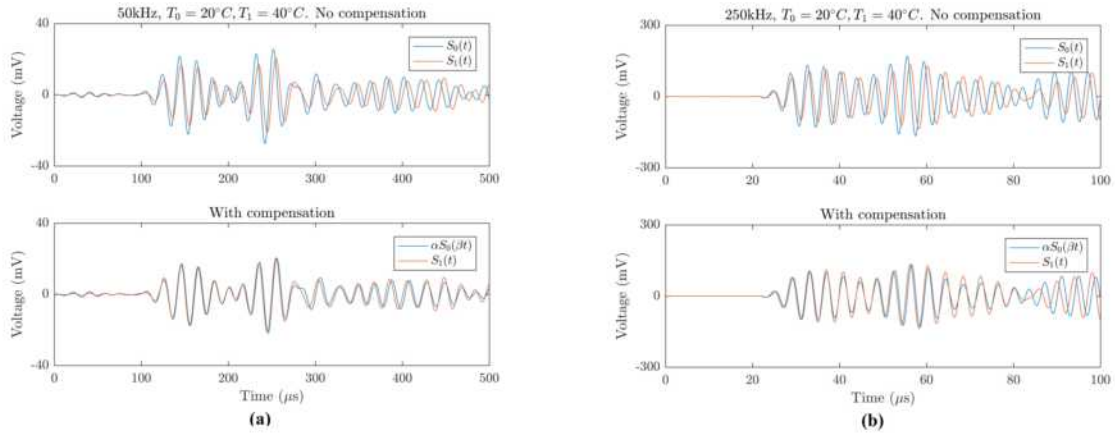

Figure 7: Temperature compensation of the signal recorded in path A2S8 from Panel A. Signal S_0 was recorded at $T_0 = 20°C$. Signal S_1 was recorded at $T_1 = 40°C$. The figure above plots the two signals and the figure below plots the compensated signal S_0, $\alpha S_{T_0}(\beta t)$, with S_1. (a) Response to 50kHz 5-cycle toneburst excitation. (b) Response to 250kHz 3-cycle toneburst excitation.

Figure 7 shows the signals recorded in path A2S8 of panel A (Figure 1) before and after compensation. It can be seen that the wave dispersion behaviour is more significant at the 250kHz than at 50kHz. For signal at 50 kHz the shape of the wave is similar to the excitation signal in the direct arrival wave packet and the first boundary reflected wave packet, while prolonged wave packets can be seen at 250 kHz. For the signal response to 50kHz excitation, the amplitude and phase of the compensated signal $\alpha S_0(\beta t)$ lines up well with signal $S_1(t)$ in not only the first wave packet but also in the second wave packet. For the response to 250kHz excitation, the phase of the compensated signal $\alpha S_0(\beta t)$ matches well with signal $S_1(t)$ in the first two wave packets, while the amplitude only matches at the beginning of the first two wavepackets. The discrepancy in signal amplitude after compensation at 250kHz might be attributed to the change in the shape of the signal due to wave dispersion.

As discussed in section 2, the amplitude compensation factor might be dependent on the wave propagation distance due to the influence of temperature on damping. This dependence is indirectly examined by applying the amplitude compensation factor to a signal path (path A2S8) that is twice as long as the path (path A1S2) from which the amplitude compensation factor was determined. The effective amplitude compensation at both frequencies indicates that thermal effect on damping is not significant and might be neglected within the considered temperature range.

5. Experimental implementation and validation

In this section, the temperature compensation technique is implemented in two typical aircraft structures, a flat panel and a stiffened panel. The fabrication of these structures and the installation of the transducers were described in Section 3. Figure 8 shows the CFRP panel with 8 surface mounted DuraAct sensors. The dimension of the plate is $300mm \times 225mm \times 2.5mm$. A Barely Visible Impact Damage (BVID) was introduced by a drop weight impact of 20J energy at the center of the panel. Figure 9 shows the stiffened CFRP composite panel with 8 surface mounted DuraAct sensors. The dimension of panel is $500mm \times 250mm \times 2.5mm$. A 500 mm long stiffener with omega (Ω) cross-section is attached at the centre panel. A weight was dropped at the foot of the stiffener to create a 30J impact, inducing BVID.

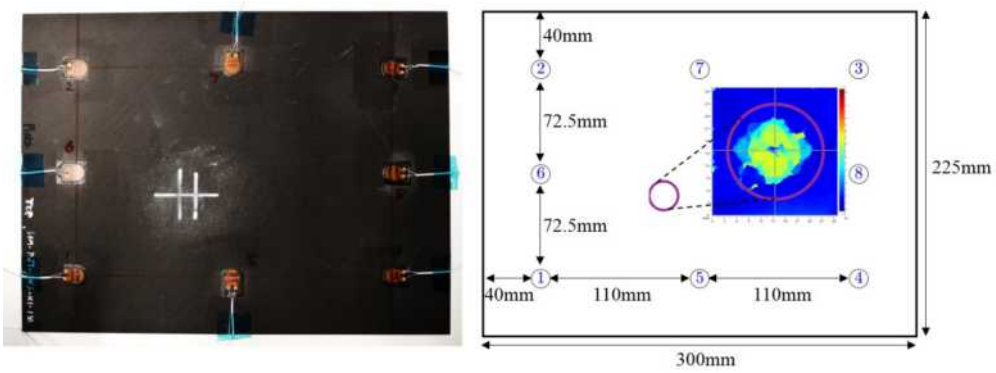

Figure 8: Panel B with 8 surface mounted DuraAct transducers

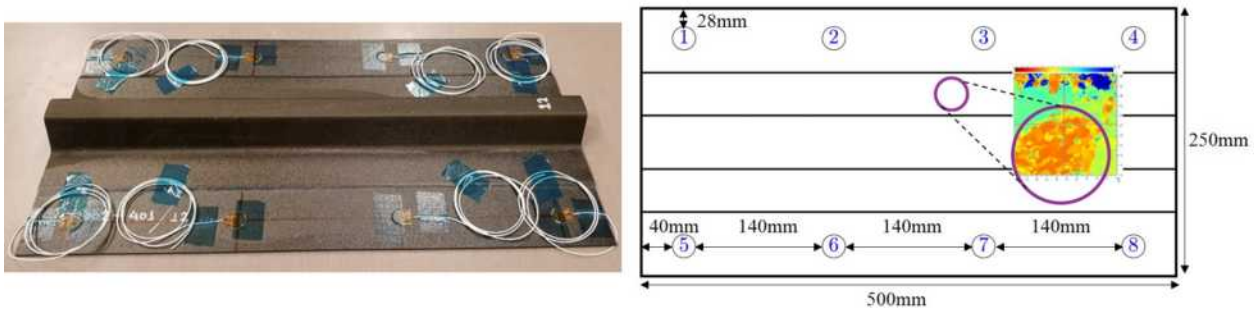

Figure 9: Panel C with 8 surface mounted DuraAct transducers

Signals were recorded from the two panels in an environmental chamber from 20°C to 45°C at every 5°C before the impact. Previously obtained compensation factors from Panel A (shown in Figure 6) in the respective directions were used to compensate the temperature effect on the toneburst signals measured from Panel B and C.

Figure 10 shows the compensation results for panel B from signal path A1S5 in the similar manner to Figure 7. Even though the first wavepacket overlaps with multiple boundary reflected wavepackets, the phase difference between the two signals is well compensated for the first two wave packets of the signal length at both 50kHz and 250kHz. The amplitude difference is almost entirely eliminated for signal at 50 kHz and is compensated at the beginning of the signal at 250kHz.

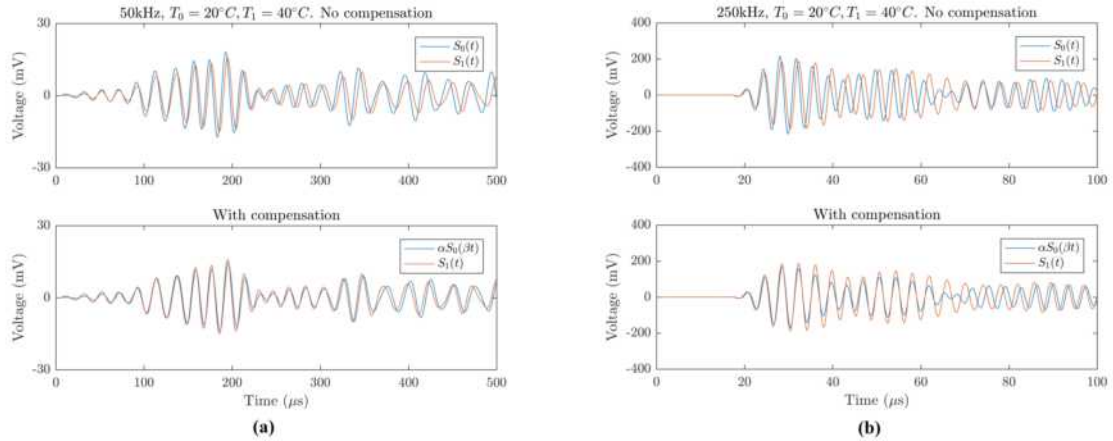

Figure 10: Temperature compensation of the signal recorded in path A1S5 from Panel B. Signal S_0 was recorded at $T_0 = 20°C$. Signal S_1 was recorded at $T_1 = 40°C$. The figure above plots the two signals and the figure below plots the compensated signal S_0, $\alpha S_{T_0}(\beta t)$, with S_1. (a)Response to 50kHz 5-cycle toneburst excitation. (b) Response to 250kHz 3-cycle toneburst excitation.

For the stiffened panel C, two signal paths are shown considering the effect of the stiffener on signal propagation. Figure 11 shows the signals from path A2S3 on the same side of the stiffener. Despite being prone to superposition of the reflected wave from the edge of the panel and the edge of the stiffener, the shape of the signals remain similar to those in the simple panels and the first arrival of the two wave modes can still be clearly spotted. Temperature compensation results obtained are also similar to the results in panel B shown in Figure 10. Figure 12 shows the signals from path A2S6 which crosses the stiffener. The form of the signals changed significantly at both frequencies, which is due to the guided wave scattering, attenuation as well as mode conversion at the stiffener. The drop of signal amplitude is more significant at 250kHz than 50kHz. Despite the significant change of the guided wave signal across the stiffener, the compensation method is still able to partially correct the signal amplitude and phase, although not as effective for the signal recorded from the same side of the stiffener.

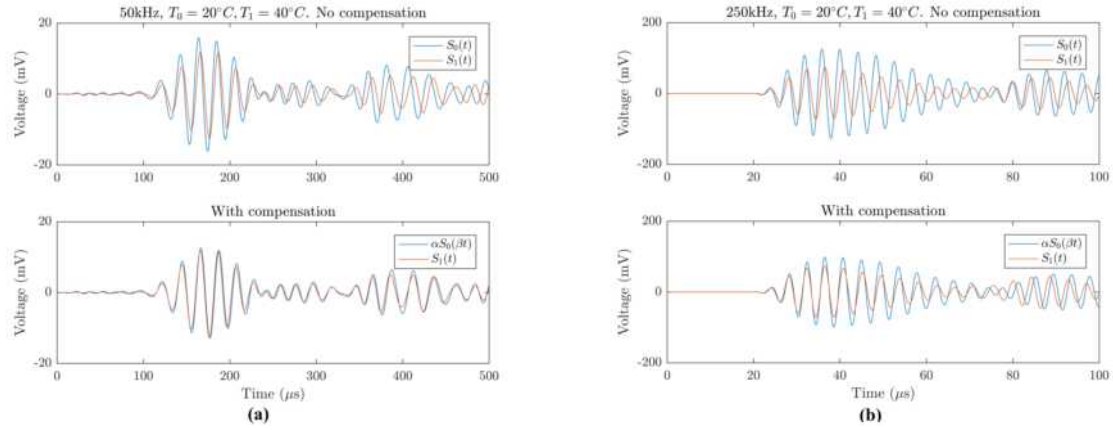

Figure 11: Temperature compensation of the signal recorded in path A2S3 from Panel C. Signal S_0 was recorded at $T_0 = 20°C$. Signal S_1 was recorded at $T_1 = 40°C$. The figure above plots the two signals and the figure below plots the compensated signal S_0, $\alpha S_{T_0}(\beta t)$, with S_1. (a) Response to 50kHz 5-cycle toneburst excitation. (b) Response to 250kHz 3-cycle toneburst excitation.

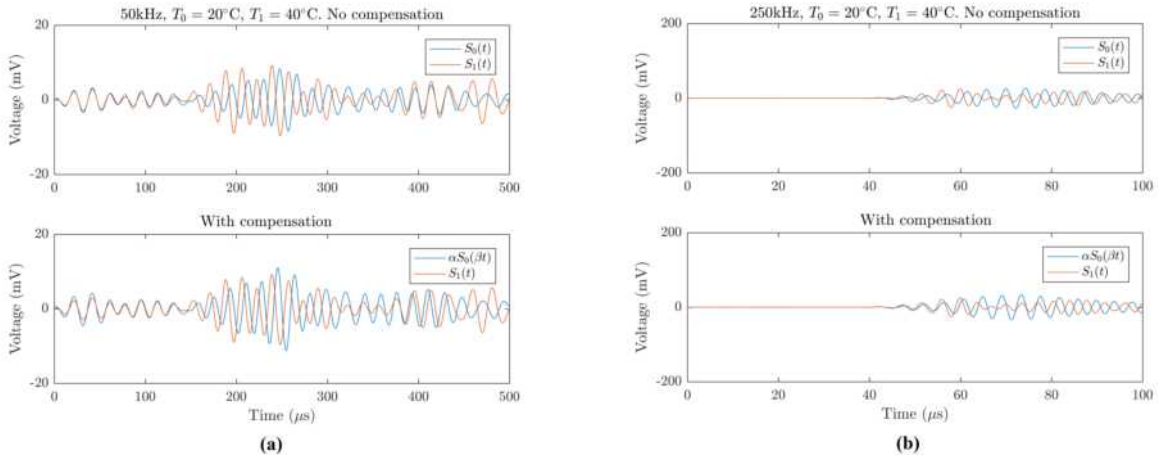

Figure 12: Temperature compensation of the signal recorded in path A2S6 from Panel C. Signal S_0 was recorded at $T_0 = 20°C$. Signal S_1 was recorded at $T_1 = 40°C$. The figure above plots the two signals and the figure below plots the compensated signal S_0, $\alpha S_{T_0}(\beta t)$, with S_1. (a) Response to 50kHz 5-cycle toneburst excitation. (b) Response to 250kHz 3-cycle toneburst excitation.

In both panels, the temperature compensation technique is more effective for signals at 50kHz than for signals at 250kHz due to the less dispersive behaviour of the guided wave at 50kHz than that at 250kHz. Here 50kHz excitation is selected to be used for damage diagnostic because: (1) the temperature effect on the signal can be better compensated and (2) the A0 mode dominant at 50kHz is more sensitive to de-lamination than S0 mode dominant at 250kHz [24].

5.1. Damage detection

After impact damage is introduced in both panels, signals were recorded again in a thermal chamber from 20°C to 45°C at every 5°C. The signal recorded before impact at 20°C was used as the baseline signal. All the other signals are used as current signals. The degree of match of a baseline signal and a current signal is evaluated using the Normalised Residual Amplitude (NRA) as:

$$NRA = \frac{\max|S_c(t) - S_b(t)|}{\max|S_b(t)|} \tag{21}$$

where $S_c(t)$ is the current signal and $S_b(t)$ is the baseline signal. In order to eliminate the influence of boundary reflection waves, only the first wave packet of the signal is taken into account. The peak of the first wave packet is identified with the envelope of the signal obtained using the magnitude of the Hilbert transform of the signal. The time window of the first wavepacket is then set to half of the excitation signal time before and after the time of the peak of the first wavepacket.

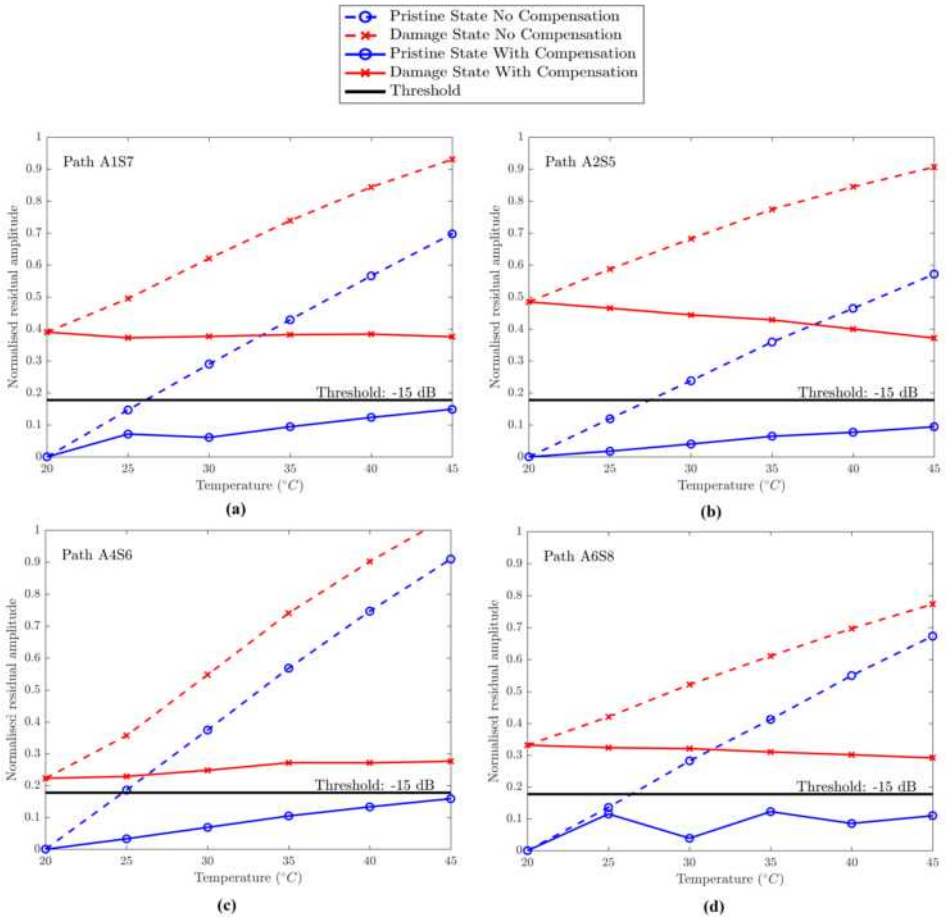

Figure 13: Normalised residual amplitudes of panel B (Figure 8) for pristine and damaged state guided wave response to 50 kHz toneburst excitation at multiple temperature conditions. Baseline signal temperature is 20°C.

Figure 13 shows the normalised residual amplitude of four signal paths on panel B (Figure 8) for the pristine state and the damaged state under multiple temperature conditions. To distinguish between the pristine state and the damaged state, the normalised residual amplitude at two states must be at different value range[16]. With temperature compensation on the baseline signal, the normalised residual amplitude for the pristine and damaged states were both reduced, and a threshold of -15 dB can be drawn to separate the two states.

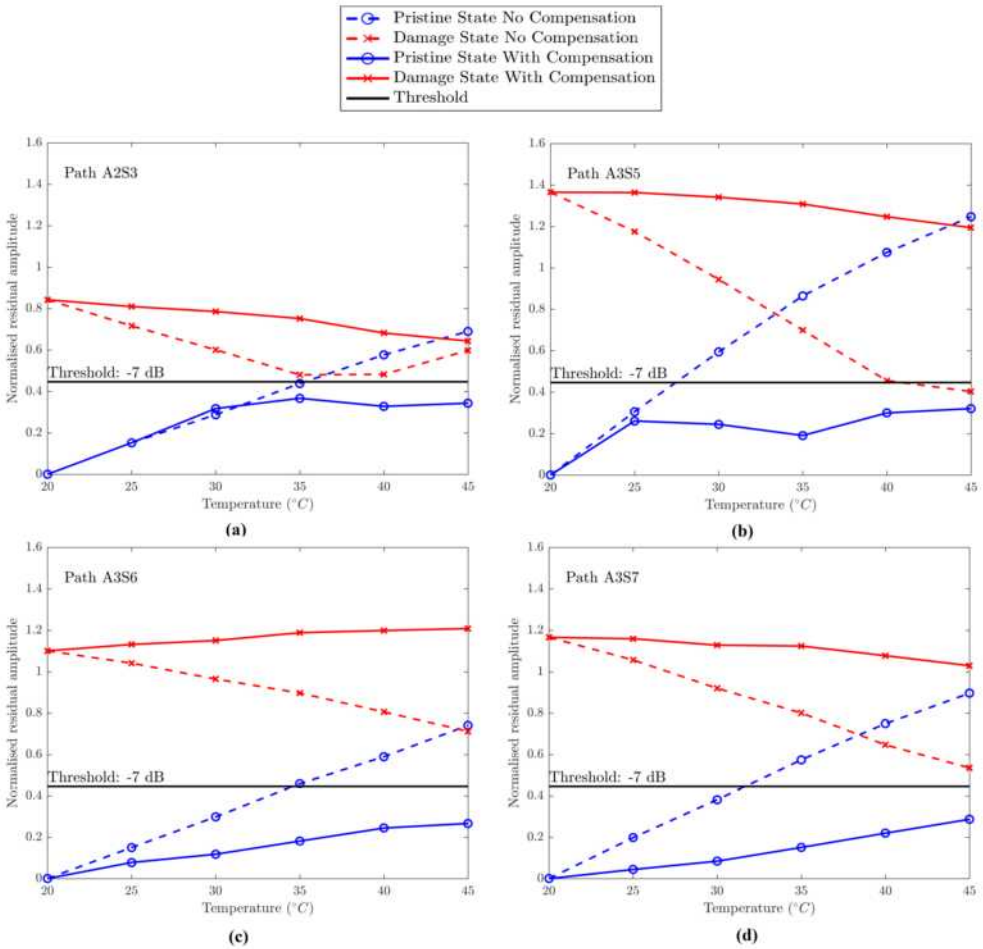

Figure 14: Normalised residual amplitude of the stiffen panel (Figure 9) at pristine state and damage state A0 mode guided wave response to 50 kHz toneburst excitation at a multiple temperature conditions. Baseline signal temperature is 20°C.

Figure 14 shows the normalised residual amplitude of four signal paths on panel C (Figure 9) for the pristine state and damaged state under multiple temperature conditions. With temperature compensation on the baseline signal, the normalised residual amplitude for the pristine and damaged states were both reduced, and a threshold of -7 dB can be drawn to separate the two states.

5.2. Damage localisation

The proposed temperature compensation method is also implemented in the localisation of the damage using delay and sum algorithm [1]. Delay and sum algorithm imaging relates the locations on a structure to the positions in recorded signal vector. The corresponding time position η to coordinates $\boldsymbol{x}$ is

$$\eta(\boldsymbol{x}) = \frac{D_{A-\boldsymbol{x}}./v_{A-\boldsymbol{x}} + D_{\boldsymbol{x}-S}./v_{\boldsymbol{x}-S} + t_{off}}{f_s} \tag{22}$$

where D is the propagation distance, v is group velocity corresponding to the path direction determined in Figure 2, t_{off} is time lag counting for the delays in acquisition system, f_s is the sampling frequency of the acquisition channel. Likelihood of the coordinate $\boldsymbol{x}$ being the location of damage is:

$$I(\boldsymbol{x}) = \frac{1}{\sum_i r_i[\eta(\boldsymbol{x})])} \tag{23}$$

where r_i is the residual signal vector of path i. Neighbourhood image processing is implemented to eliminate the outliers of likelihood value at scattered location. Mean filter is applied at each of the locations $\boldsymbol{x}$. The

estimated damage location is then determined as

$$\hat{\boldsymbol{x}} = argmax I(\boldsymbol{x}) \tag{24}$$

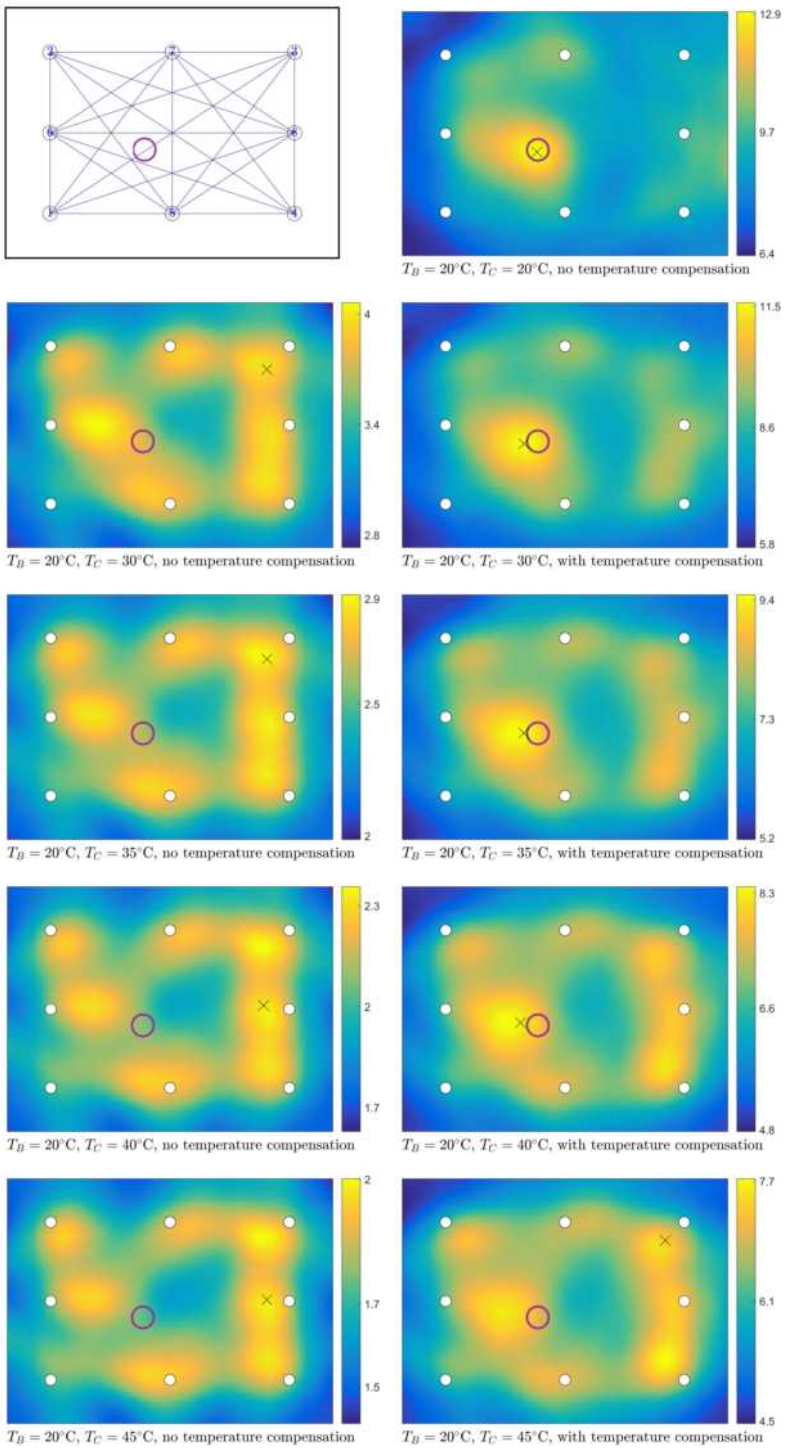

Figure 15: Damage localisation for panel B using A0 mode guided wave response to 50 kHz toneburst excitation at various temperature conditions. The purple circle marks the actual damage location, the cross marks the predicted damage location.

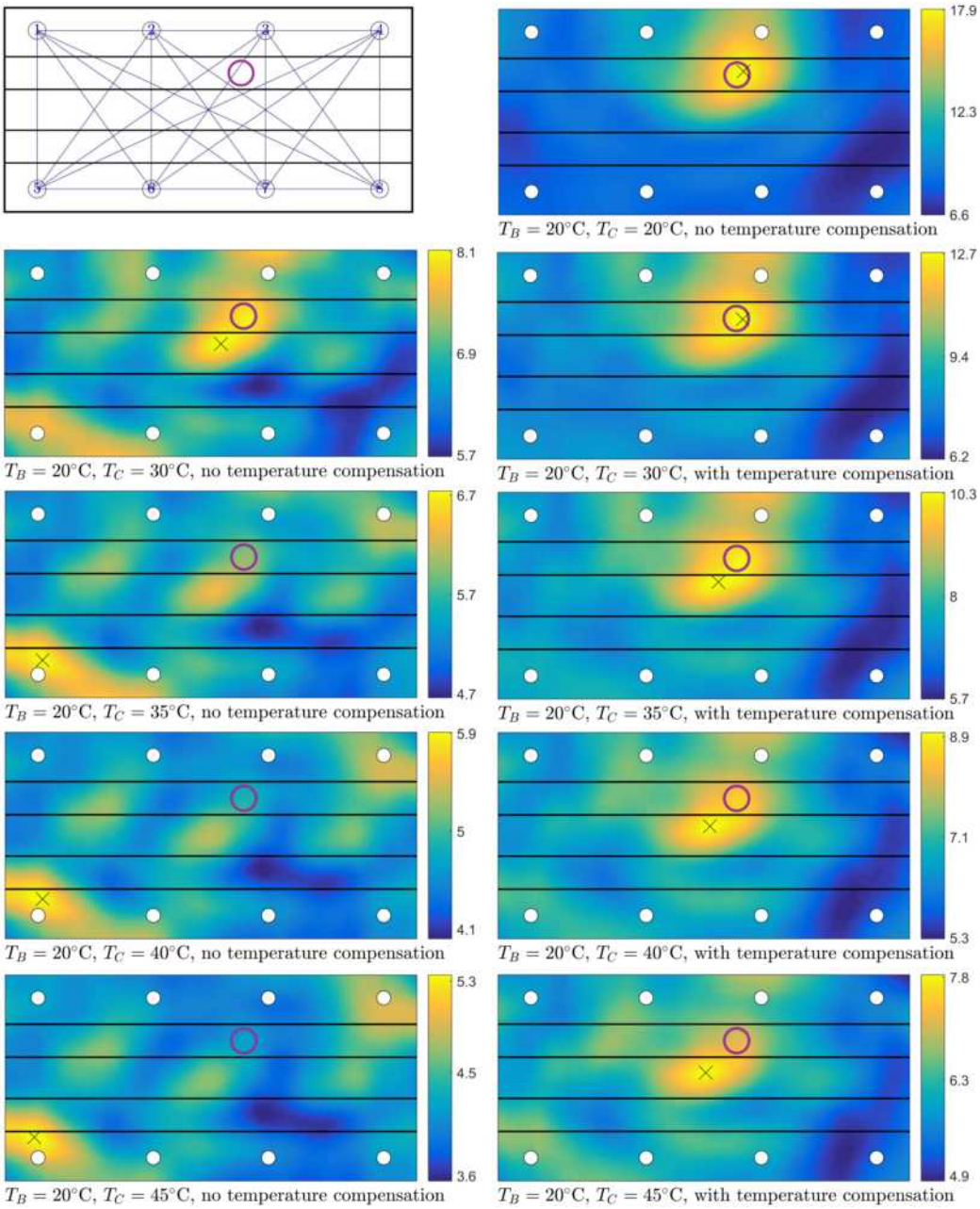

Figure 16: Damage localisation for panel C using A0 mode guided wave response to 50 kHz toneburst excitation at various temperature conditions.The purple circle marks the actual damage location, the cross marks the predicted damage location.

Figure 15 and Figure 16 present the localisation results for panel B and panel C, respectively. All the possible signal path are used for damage imaging. Path network diagrams are shown on the top left of Figure 15 and Figure 16. The localisation results for the signals corresponding to the pristine and damaged states at 20°C are shown for reference to the results obtained with pristine and damaged signals at different temperatures. The damage state signal at 30°C, 35°C, 40°C and 45°C are used with pristine state signal at 20°C as baseline. Without temperature compensation, the localisation results deteriorate as the damaged state temperature deviates from the baseline temperature for both panels. When temperature compensation is implemented, the localisation result can be restored to nearly the unimpaired result provided that the current temperature is less than 20°C higher than the baseline temperature.

Damage localisation results for panel C obtained with current temperature lower than the baseline temperature are also shown in Figure 17. The current state signal recorded at 10°C, 5°C, 0°C and -5°C are used with

pristine state signal at 20°C as baseline. It can be seen that the deterioration of the localisation result due to temperature variation can be corrected using the proposed temperature compensation approach given that the current temperature is no more than 20°C lower than the baseline temperature.

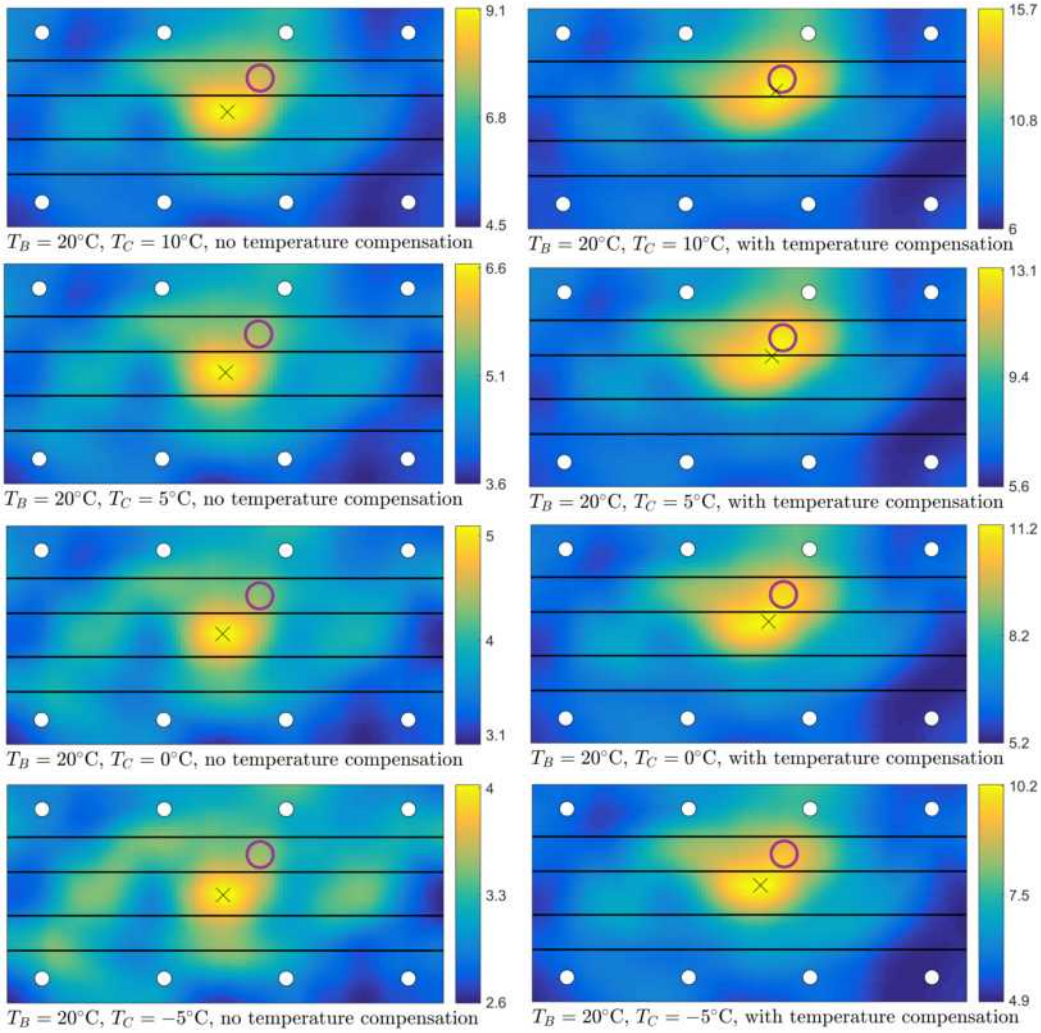

Figure 17: Damage localisation for panel C using S0 mode guided wave response to 50 kHz toneburst excitation at various temperature conditions. The purple circle marks the actual damage location, the cross marks the predicted damage location.

6. Discussion

The proposed temperature baseline reconstruction approach has been examined through the match of the signals, detection and localisation of barely visible impact damage in anisotropic composite structures. Despite the effective performance, the propose method does have certain limitations that need further investigation and are considered in the future scope of our work.

Nearly perfect match of the reconstructed baseline signal with the recorded baseline signal is achieved for A0 mode, while good match is obtained at the beginning of the signal for S0 mode, as shown in Figure 7, 10 and 11. The reason for this different effectiveness of the proposed method for the two wave mode lies behind the consideration of the dispersive nature of guided wave. The A0 mode response shown in this work is nearly non-dispersive within the tested temperature range, and thus the deviation of the signal due to temperature change can be effectively compensated. The S0 mode response, however, is highly dispersive and the shape of the signal changes significantly for the tested temperature range. As the derivation of the compensation factor

assumes non-dispersive guided wave response, the reconstructed S0 mode signal shows greater mismatch to the experimental observation.

In this work the compensation factors used in the stiffened panel C are the same as the factors used in the simple flat panel B, which is the key idea of a readily applicable temperature compensation approach to larger structure with added structural complexity. As shown in Figure 14, 16 and 17, despite the additional structural complexity caused by the stiffener, the compensation factors worked well in detecting and locating barely visible impact damage in panel C. However, the stringer does indeed change the wave mode, amplitude and phase of the guided wave significantly, as shown in Figure 12. As can be seen from Figure 12, the compensation results for the signal path across the stiffener is not as good as those for the signal paths that do not cross the stiffener. The effect of stiffener on the signal under varying thermal conditions needs to be further studied in order to better compensate the temperature effect in complex structures.

7. Conclusion

In this work a physical based temperature baseline reconstruction approach for guided wave structural health monitoring in anisotropic composite structures is presented. The effects of temperature on signal amplitude and arrival time are investigated and quantified as dimensionless amplitude and arrival time factors. Both factors show significant dependence on signal path orientation. As a result, these factors are expressed as functions of this orientation as well as temperature difference, allowing this technique to be conveniently applied to baseline reconstruction in anisotropic structures. In addition, by deriving dimension independent compensation factors, those derived for simple structures can be easily applied to other structures of larger size and increased complexity, provided the structures are composed of the same material and installed with the same type of sensors.

To account for the temperature effect on signals, a significant amount of pristine signals typically need to be collected over a large temperature range to serve as a library of signals at all possible temperatures. With the help of this novel temperature compensation technique, the effect of temperature difference can be compensated, and less baseline data is required. Therefore, the implementation of GWSHM systems on structures of large size and significant complexity can be more efficiently carried out.

The derived compensation factors are shown to be effective in compensating the temperature effect of signals in two typical aerospace composite structures, a flat panel and a stiffened panel. Using baseline signals recorded at 20°C and the corresponding compensation factors, impact damage is distinguished by a set threshold for current state signal at up to 45°C. Good damage localisation results are achieved for current state signals for temperature differences of up to 20°C from the baseline signal.

8. Acknowledgements

This work is part of complementary research contributing to SHERLOC Project. SHERLOC project is coordinated by the Structural Integrity and Health Monitoring group of Imperial College London.

References

[1] Michaels, Jennifer E. and Michaels, Thomas E. Guided wave signal processing and image fusion for in situ damage localization in plates. *Wave Motion*, 44(6):482–492, 2007.

[2] Xiaoliang Zhao, Huidong Gao, Guangfan Zhang, Bulent Ayhan, Fei Yan, Chiman Kwan, and Joseph L. Rose. Active health monitoring of an aircraft wing with embedded piezoelectric sensor/actuator network: I. defect detection, localization and growth monitoring. *Smart Materials and Structures*, 16(4):1208–1217, 2007.

[3] E. B. Flynn, M. D. Todd, P. D. Wilcox, B. W. Drinkwater, and A. J. Croxford. Maximum-likelihood estimation of damage location in guided-wave structural health monitoring. *Proceedings of the Royal Society A: Mathematical, Physical and Engineering Sciences*, 467(2133):2575–2596, 2011.

[4] Eric B Flynn, Michael D Todd, Anthony J Croxford, Bruce W Drinkwater, and Paul D Wilcox. Enhanced detection through low-order stochastic modeling for guided-wave structural health monitoring. *Structural Health Monitoring*, 11(2):149–160, 2012.

[5] Z. Sharif-Khodaei and M. H. Aliabadi. Assessment of delay-and-sum algorithms for damage detection in aluminium and composite plates. *Smart Materials and Structures*, 23(7):075007, 2014.

[6] Z. Sharif-Khodaei and M. H. Aliabadi. Lamb-wave based damage detection in anisotropic composite plates. *Key Engineering Materials*, 627:1–4, 2014.

[7] Fangxin Zou, Jing Rao, and M.H. Aliabadi. Highly accurate online characterisation of cracks in plate-like structures. *NDT & E International*, 94:1 – 12, 2018.

[8] G Konstantinidis, BW Drinkwater, and PD Wilcox. The temperature stability of guided wave structural health monitoring systems. *Smart Materials and Structures*, 15(4):967, 2006.

[9] Yinghui Lu and Jennifer E Michaels. A methodology for structural health monitoring with diffuse ultrasonic waves in the presence of temperature variations. *Ultrasonics*, 43(9):717–731, 2005.

[10] Anthony J Croxford, Jochen Moll, Paul D Wilcox, and Jennifer E Michaels. Efficient temperature compensation strategies for guided wave structural health monitoring. *Ultrasonics*, 50(4):517–528, 2010.

[11] Joel B Harley and José MF Moura. Scale transform signal processing for optimal ultrasonic temperature compensation. *IEEE transactions on ultrasonics, ferroelectrics, and frequency control*, 59(10):2226–2236, 2012.

[12] Ziemowit Dworakowski, Lukasz Ambrozinski, and Tadeusz Stepinski. Multi-stage temperature compensation method for lamb wave measurements. *Journal of Sound and Vibration*, 382:328–339, 2016.

[13] Guoqiang Liu, Yingchun Xiao, Hua Zhang, and Gexue Ren. Baseline signal reconstruction for temperature compensation in lamb wave-based damage detection. *Sensors*, 16(8):1273, 2016.

[14] Francesco Lanza di Scalea and Salvatore Salamone. Temperature effects in ultrasonic lamb wave structural health monitoring systems. *The Journal of the Acoustical Society of America*, 124(1):161–174, 2008.

[15] Surajit Roy, Kuldeep Lonkar, Vishnuvardhan Janapati, and Fu-Kuo Chang. A novel physics-based temperature compensation model for structural health monitoring using ultrasonic guided waves. *Structural Health Monitoring*, 13(3):321–342, 2014.

[16] Claude Fendzi, Marc Rebillat, Nazih Mechbal, Mikhail Guskov, and Gérard Coffignal. A data-driven temperature compensation approach for structural health monitoring using lamb waves. *Structural Health Monitoring*, 15(5):525–540, 2016.

[17] AJ Croxford, PD Wilcox, BW Drinkwater, and G Konstantinidis. Strategies for guided-wave structural health monitoring. In *Proceedings of the Royal Society of London A: Mathematical, Physical and Engineering Sciences*, volume 463, pages 2961–2981. The Royal Society, 2007.

[18] Matthieu Gresil and Victor Giurgiutiu. Prediction of attenuated guided waves propagation in carbon fiber composites using rayleigh damping model. *Journal of Intelligent Material Systems and Structures*, 26(16): 2151–2169, 2015.

[19] Konstantin J Schubert and Axel S Herrmann. On the influence of moisture absorption on lamb wave propagation and measurements in viscoelastic cfrp using surface applied piezoelectric sensors. *Composite Structures*, 94(12):3635–3643, 2012.

[20] Westin B Williams, Thomas E Michaels, and Jennifer E Michaels. Characterization of guided wave velocity and attenuation in anisotropic materials from wavefield measurements. In *AIP Conference Proceedings*, volume 1706, page 030002. AIP Publishing, 2016.

[21] Nan Yue, Zahra Sharif Khodaei, and Ferri M.H. Aliabadi. An innovative secondary bonding of sensors to composite structures for shm application. In *Advances in Fracture and Damage Mechanics XVII*, volume 774 of *Key Engineering Materials*, pages 516–522. Trans Tech Publications Ltd, 9 2018. doi: 10.4028/www.scientific.net/KEM.774.516.

[22] Jennifer E Michaels, Sang Jun Lee, Anthony J Croxford, and Paul D Wilcox. Chirp excitation of ultrasonic guided waves. *Ultrasonics*, 53(1):265–270, 2013.

[23] Sungwon Ha, Kuldeep Lonkar, Amrita Mittal, and Fu-Kuo Chang. Adhesive layer effects on pzt-induced lamb waves at elevated temperatures. *Structural Health Monitoring*, 9(3):247–256, 2010.

[24] MS Salmanpour, Z Sharif Khodaei, and MH Aliabadi. Guided wave temperature correction methods in structural health monitoring. *Journal of Intelligent Material Systems and Structures*, 28(5):604–618, 2017.